Association for Information and Image Management
1100 Wayne Avenue, Suite 1100
Silver Spring, Maryland 20910
301/587-8202

Centimeter

1 2 3 4 5 6 7 8 9 10 11 12 13 14 15 mm

1 2 3 4 5

Inches

1 of 1

KAPL-4763

STRESS CORROSION CRACK TIP MICROSTRUCTURE IN NICKEL-BASE ALLOYS

S. A. Shei and W. J. Yang

Prepared For:

Corrosion/94 Symposium
Baltimore, MD
February 28 - March 5, 1994

KNOLLS ATOMIC POWER LABORATORY
SCHENECTADY, NEW YORK

DISCLAIMER

CONTENTS

TABLES

ILLUSTRATIONS

ILLUSTRATIONS (Continued)

ILLUSTRATIONS (Continued)

STRESS CORROSION CRACK TIP MICROSTRUCTURE IN NICKEL-BASE ALLOYS*

S.A. Shei and W.J. Yang
Knolls Atomic Power Laboratory
Martin Marietta Corporation
PO Box 1072
Schenectady, NY 12301

ABSTRACT

Stress corrosion cracking behavior of several nickel-base alloys in high temperature caustic environments has been evaluated. The crack tip and fracture surfaces were examined using Auger/ ESCA and Analytical Electron Microscopy (AEM) to determine the near crack tip microstructure and microchemistry. Results showed formation of chromium-rich oxides at or near the crack tip and nickel-rich de-alloying layers away from the crack tip. The stress corrosion resistance of different nickel-base alloys in caustic may be explained by the preferential oxidation and dissolution of different alloying elements at the crack tip. Alloy 600 (UNS N06600) shows good general corrosion and intergranular attack resistance in caustic because of its high nickel content. Thermally treated Alloy 690 (UNS N06690) and Alloy 600 provide good stress corrosion cracking resistance because of high chromium contents along grain boundaries. Alloy 625 (UNS N06625) does not show as good stress corrosion cracking resistance as Alloy 690 or Alloy 600 because of its high molybdenum content.

Keywords: stress corrosion cracking, Alloy 600, Alloy 690, Alloy 625, nickel-base alloys, caustic, high temperature water, crack tip, microstructure.

INTRODUCTION

Nickel-chromium alloys are generally used for their superb corrosion resistance and excellent fabricability. Alloy 600 (UNS N06600) and Alloy 690 (UNS N06690) have been used widely for nuclear power applications. [1-4] Alloy 600 has been tested extensively regarding its stress corrosion cracking (SCC) resistance because of the SCC problems encountered in the nuclear power plants. Thermally treated Alloy 690 has shown improved SCC resistance relative to Alloy 600 in laboratory testing and is regarded as the tubing material for new or replacement steam generators for nuclear power applications. Alloy 625 (UNS N06625) has good SCC resistance [5] and has been used in chemical processing, nuclear and aerospace fields. It can also be heat treated to achieve significantly higher strength than Alloy 600 or Alloy 690. [6] However, laboratory test results to date have shown SCC susceptibility of these three alloys in strong caustic environments. [7] Although SCC test results of these alloys in caustic environments have been available for many years, there is only limited information regarding corrosion behavior and microstructure near the crack tip. Auger electron spectroscopy analyses, performed on tube surfaces of Alloy 600 and Alloy 690 tubing after exposure in 10 and 50% caustic solutions containing 1% Na_2CO_3, showed a nickel (Ni)-rich surface layer with de-alloying of chromium (Cr) and iron (Fe). [8] Auger/ESCA analyses, performed on fracture surfaces of Alloy 600 tubing after exposure in 10% caustic solutions, indicated that the surface layers were enriched in Ni and depleted in Cr at the crack opening, mid crack and crack tip. [9] The crack tip of Alloy 600 tubing after exposure in a 10% caustic solution was evaluated using Analytical Electron Microscopy (AEM). [10] The results showed Cr-rich oxides near the crack tip and no Ni-rich de-alloying surface layers. This study evaluates the crack tip microstructure and corrosion products inside the cracks of Alloy 625, Alloy 600 and Alloy 690 using AEM and Auger/ESCA. This information will help to provide better understanding of the stress corrosion cracking phenomenon in these Ni-base alloys.

EXPERIMENTAL PROCEDURES

The materials tested consisted of Alloys 625, 690 and 600 tubes and Alloy 625 plates. The compositions of the these nickel-base alloys are provided in Table 1. All tubing materials were mill annealed. Split tube U-bend specimens (STUB) were fabricated from the tubing materials. The specimens were bent using a one inch diameter mandrel. The spread between two legs was increased to 1.6 times springback after bending to apply a tensile stress on the tube OD surface. This resulted in approximately 16% strain on the OD surface. All tubing blanks were stress relieved prior to bending. Alloy 600 specimens were stress relieved at 607°C and Alloy 625 tubing specimens were stress relieved at 566°C. For the Alloy 690 specimens, a 1052°C /718°C thermal treatment was performed before the 607°C/566°C stress relief heat treatment. For the Alloy 625 plate, single U-bend (SUB) specimens were used. SUB blanks were thermally treated at 1093°C/871°C/649°C and stress relieved at 566°C prior to bending. These SUB specimens were bent using a 3/4 inch diameter mandrel. This resulted in up to 17% strain on the edge surface. The thermal histories of these materials are provided in Table 2.

Stress corrosion cracking testing was conducted in a nickel autoclave. The tests were conducted in a deaerated, static 10% NaOH solution at 307°C. Specimens were exposed for 500 hours and were then removed and rinsed in de-ionized water after testing. Metallographic specimens were mounted and polished to evaluate the crack morphology and the average maximum crack depth.

Auger/ESCA evaluations of surface films on exposed surfaces and crack facets were performed. Specimens for AEM evaluation were sectioned near the crack tip by the method shown in Figure 1. Thin foils were prepared through a series of grinding, dimpling and ion milling to preserve the corrosion products and microstructure near the crack tip. The most crucial step in specimen preparation was a careful mechanical dimpling of the crack tip region. The final thinning was done by argon ion erosion milling in a GATAN ion-miller. The ion milling was performed using a liquid nitrogen cold stage to minimize any surface contamination and changes in microstructure or corrosion products during specimen preparation.

RESULTS

Stress corrosion cracking occurred in all three alloys after 500 hours exposure. The maximum crack depth was measured in each specimen on metallographic cross-sections near the mid-thickness position. The average maximum crack depth, which was an average of the maximum crack depths observed in two or more specimens, was used to provide a relative ranking of SCC resistance. Alloy 625, which had the largest crack depth, showed more severe cracking than Alloys 690 and 600. Alloy 690 had slightly smaller crack depths compared to Alloy 600. Table 2 provides the average maximum crack depths for different materials tested. The differences in SCC resistance and its correlation with microstructural evaluations are discussed below.

SEM Evaluation

General Surfaces. Specimens were evaluated using scanning electron microscopy (SEM) after 500 hours exposure in 10% caustic. Micrographs of general surfaces of Alloy 600, Alloy 690 and Alloy 625 are shown in Figure 2. Alloy 600 showed the least corrosion attack. There was no obvious grain boundary attack and the surface grinding marks remained visible on the Alloy 600 tube OD surface. Alloy 690 tubing showed preferential grain boundary attack and grain boundaries were well delineated. Alloy 625 showed more severe general attack with some preferential grain boundary attack. The grain boundaries were not as well delineated as those of Alloy 690.

SCC Crack Facets. Intergranular cracking was generally observed for Alloy 625, Alloy 600 and Alloy 690 specimens. A more detailed evaluation was performed on the Alloy 625 specimen. An SEM micrograph of crack facets of an Alloy 625 specimen is shown in Figure 3. Figure 4 shows a layer of corrosion products on the crack facets. Energy Dispersive X-ray spectra analysis (EDX) showed enrichment of Cr and Ti in the corrosion products, compared with the base Alloy 625 composition.

Auger/ESCA Analysis

General Surfaces. Auger/ESCA analyses of Alloys 600, 690 and 625 showed Ni enrichment on the general corrosion surface. Figure 5 shows Auger results of an Alloy 625 specimen. The surface was enriched in Ni and depleted in Mo, Cr, Nb and Fe. ESCA results showed that the primary corrosion products near the surface layer were $Ni(OH)_2$ and Cr(III) based spinel or oxide, Figure 6. Underneath this layer, Cr(III) based spinels or oxides were the main corrosion products.

Fe(III) and Fe(II) based spinels or oxides were also present in small quantities. Similar Auger results were observed for Alloy 600 and Alloy 690. Figures 7 and 8 show that the general corrosion surfaces are enriched in Ni and depleted in Cr and Fe for both Alloy 600 and Alloy 690. ESCA results showed primary corrosion products as $Ni(OH)_2$, a Cr(III) based spinel (or oxide) and a Ni(II) based spinel (or oxide).

SCC Crack Facets. The surface film composition of the crack facets near the crack tip was evaluated using Auger analysis. Figure 9 shows the Auger results for Alloy 625. Unlike the general corrosion surface, the fracture surface near the crack tip showed enrichment in Cr and Ti. It was depleted in Mo, Ni and, to a lesser extent, Fe and Nb. The oxide layer was thicker than that on the general surface. The reason for the apparent Cr-enrichment probably comes from the Cr-rich oxides inside the crack tip which covers part of the crack facets. This is confirmed by AEM results inside the crack tip, as discussed in the next section. Figure 10 shows the Auger results of crack facets near the crack opening. It showed enrichment in Ni and depletion in Cr, Mo, Nb and Fe. This is similar to the general corrosion surface film composition. Auger results of Alloys 600 and 690 were similar to the Alloy 625 results. The crack facets near the crack tip of Alloy 600 and Alloy 690 showed enrichment in Cr and Ti, Figures 11 and 12. The crack facets near the crack opening showed enrichment in Ni, similar to the general corrosion surface.

AEM Evaluation

Thin foils for AEM evaluations were prepared from the Alloy 625 SUB specimen of plate Heat B. The electron transparent area in the thin foil prepared revealed two kinds of cracks as shown in the enlarged view in Figure 13. One is a primary crack and another is a branched, secondary crack. The observations along the crack depth are given by regions illustrated in Figure 13.

Crack Opening (Region 1). Inside the crack opening, but near the crack mouth, a continuous, Ni-rich de-alloying layer (~ 15 nm wide) was observed on the crack surface, Figure 14. Two types of corrosion products were found inside the crack opening. One appeared as acicular crystals and was enriched in Cr and Ti. The electron diffraction ring pattern of these crystals matched the rhombohedral crystal structure of the Cr_2O_3-type oxide. The oxide morphology and its diffraction ring pattern are shown in Figure 15. The electron energy loss spectra (EELS) and EDX in Figure 15 show Cr-Ti-O in these crystals. These results indicated the presence of Cr_2O_3-type oxides. The Ti-rich oxide could be $CrTiO_3$ but was not positively identified. The other corrosion product appeared as loose flakes and was identified as the Nb_2O_5 oxide.

Mid Crack (Region 2). This is a region where a small crack branched off from the main crack. A Ni-rich de-alloying layer as wide as 40 nm was observed at the mouth of the small crack. The microdiffraction pattern of the Ni-rich de-alloying layer had the same crystal orientation as the Alloy 625 matrix. This suggested that the Ni-rich de-alloying layer was part of the metal matrix. Figure 16 shows the microdiffraction patterns and the EDX spectra of the Ni-rich de-alloying layer and the metal matrix. Similar to the crack opening, the acicular Cr and Ti rich oxides were observed inside the crack. Partially dissolved Cr-rich carbides ($Cr_{23}C_6$) were also observed inside the crack. Figure 17 shows a $Cr_{23}C_6$ carbide particle inside the crack. This indicated that the grain boundary carbide ($Cr_{23}C_6$) was not consumed completely during the SCC process.

Secondary Crack Tip (Region 3). This is the crack tip of the branched crack. The corrosion products, which showed acicular crystals, were enriched in Cr-Ti-O, Figure 18. Figure 19 shows the diffraction pattern of the oxide at the crack tip region. The diffraction pattern also matched the Cr_2O_3-type crystal structure. These results suggested that the corrosion products were a combination of Cr_2O_3 and other Cr-Ti-O oxides. The Ni-rich de-alloying layer was not detected at the crack tip region. The crack looked blunt and the crack tip was ~ 0.15 μm wide. This indicates that this crack may have not been active. At the grain boundary ahead of the crack, two "microcracks" (or cavities) were observed. One was ~ 0.025 μm ahead of the blunted crack and the other was ~ 0.16 μm ahead of the crack. The EDX results show that Ni is enriched and Mo and Cr are depleted along the grain boundary between these two "microcracks", Figure 19. The cause of these "microcracks" is not clear. It might be a result of crack tunnelling. Although this is an interesting observation, this is based on one observation and needs to be confirmed.

Primary Crack Tip (Region 4). This is the crack tip region of a primary crack. The appearance of the crack tip was different from the secondary crack tip in Region 3. This primary crack tip is sharp with an arc radius of ~20 nm and the converging of the crack forms a wedge angle of ~ 22 degree, Figure 20. Similar to Region 3, "microcracks" were also observed ahead of the crack tip. The crack tip was filled with corrosion products but there were no acicular crystals. The EELS and EDX results showed that the oxides were enriched in Cr but not Ti. These corrosion products were probably the Cr_2O_3 oxide based on the electron diffraction ring pattern. The Ni-rich de-alloying layer was not detected at the crack tip region. Figure 21 provides a summary of findings near the crack tip region.

DISCUSSION

General Surface

Auger/ESCA results showed enrichment of Ni near the corroded surface in all three alloys. The observation of a Ni-rich de-alloying layer on the general corrosion surface is expected based on electro-chemical potential (ECP) - pH (Pourbaix) diagrams. Figures 22-24 show the ECP - pH diagrams for Ni, Cr and Fe in water at 288°C, respectively. [11] The pH value for the 10% NaOH environment at 307°C (585°F) is estimated to be about 11.2, as calculated by MULTEQ. Based on the potential - pH diagrams for Ni, Cr and Fe, Ni may form a protective NiO oxide film and Cr does not form a protective oxide film at pH 11.2. Thus, the general corrosion resistance of these Inconel alloys should increase with increasing Ni level. This is consistent with the experimental observation that Alloy 600 is the most corrosion resistant among these three alloys, Figure 2, because of its high Ni content (~ 70 wt.%). Figure 22 also shows small variations of pH or potential could cause Ni to form the protective NiO or soluble $Ni(OH)_3^-$ ion. This suggests that material variability, microstructural features and local chemistry variability might cause intergranular attack (IGA) or intergranular SCC in these Ni-base alloys, depending on the local pH and potential. [12]

Crack Opening

Auger results of crack facets inside the crack opening for all three alloys are similar to that of the general surface. The surface layer inside the crack opening was enriched in Ni and slightly depleted in Cr. AEM analysis of Alloy 625 showed a distinct de-alloying zone which was almost a pure Ni layer. This Ni film was shown to have the same orientation as the matrix. This suggests that

this Ni film was formed by de-alloying rather than re-precipitation. The Ni film forms as Cr and Mo preferentially diffuse out of the base metal and oxidize in the caustic environment. A layer of corrosion products containing Cr-Ti rich oxides was observed on top of the Ni film. These oxides formed as loosely attached layers in the form of acicular crystals. The morphology of these acicular crystals suggests that they formed by re-precipitation. The presence of the Cr-rich oxides indicated that the Cr oxide solubility was exceeded inside the crack. This suggests that the Cr oxide solubility in Alloy 625 may not be as high as what is shown in the Cr-water Pourbaix diagram, Figure 23. Other experimental results indicate that the Cr(III) oxide solubility in caustic may be only about 4×10^{-10} molal (0.02 ppb) at pH = 9 at 288°C. [13]

Crack Tips

Auger results from crack facets near the crack tip for all three alloys showed Cr-enrichment. The reason for the apparent Cr-enrichment probably comes from the Cr-rich oxides which cover part of the crack facets. The cross-section AEM results of Alloy 625 showed Cr-rich oxides inside the crack tip. Similar AEM results were observed in Alloy 600 after 2000 hours exposure in 10% caustic which showed Cr-rich oxides inside the crack tip. [10] Figure 25 shows a micrograph of an Alloy 600 STUB specimen near the crack tip region. A summary of the crack tip microstructure of Alloy 600 is provided in Figure 26. The Cr-rich oxide was identified as $NiCr_2O_4$-type oxides for the Alloy 600 specimen. For Alloy 625, the Cr-rich oxide was identified as Cr_2O_3-type oxides. The reason for the difference is not understood. There are obvious differences between Alloy 600 and Alloy 625 in chemical composition and microstructure. The primary carbide at grain boundaries for Alloy 600 is Cr_7C_3. For Alloy 625, the grain boundary carbides are $Cr_{23}C_6$ and $(Ni,Mo,Cr)_6C$. Both AEM results in Alloy 600 and Alloy 625 did not show a Ni-rich de-alloying film at the crack tip. If a Ni-rich de-alloying film was present at the crack tip, it would probably be relatively thin because of the short exposure time of the crack tip to the caustic solution. The spatial resolution of the AEM/EDX technique may not be able to detect it.

The presence of Cr-rich oxides (e.g. $NiCr_2O_4$-type in Alloy 600 and Cr_2O_3-type in Alloy 625) at the crack tip in these Ni-base alloys may provide an explanation for the differences in SCC resistance. Alloy 690 has a nominal composition of 60 wt% Ni and 30 wt% Cr. This compares with Alloy 600 which has nominally 72 wt% Ni and 15 wt% Cr. Although Alloy 690 has a lower Ni level and less general corrosion resistance in caustic, it has a higher Cr level and good SCC resistance. The thermally treated Alloy 690 or Alloy 600 would show further improvement in SCC resistance because of the increased Cr content at grain boundaries resulting from the Cr-rich carbide precipitation. The Cr-rich oxides may act as a passive film and control the SCC propagation by a film rupture mechanism [14] or by a dissolution process at the crack tip. [15] The Cr-rich oxides, even if not a passive film, can fill up the crack tip and limit the mass transport of the caustic solution to the crack tip. For Alloy 625, which has nominally 8-10 wt% Mo, the SCC resistance in 10 wt% caustic is not as good as Alloy 600 or Alloy 690 because Mo is readily soluble to form $HMoO_4^-$. [16]

It is interesting to note the presence of the Cr-Ti-O oxides inside the crack opening and the secondary crack tip in Alloy 625. The base metal Ti content in Alloy 625 is 0.22 wt%. The Ti content in the Cr-Ti-O oxides is 10 to 20 times higher than the bulk Ti content. It is not known if the Cr-Ti-O oxides play any important role in the SCC process. Because these oxides are not observed inside the

main crack tip, they probably do not participate directly in the SCC process at the crack tip. TiO_2 (anatase) was reported to inhibit corrosion of Ni-base alloys in caustic. It was postulated that TiO_2 could react with Ni, Cr or Fe to form a passive film, such as Ni, Fe or Cr titanate. This study showed the presence of Cr-Ti-O oxides inside the cracks in a caustic solution. It is possible that TiO_2 could improve SCC resistance of Ni-base alloys by reacting with Cr-rich oxides to form Cr-Ti-O oxides inside the crack and limits the mass transport of the caustic solution to the crack tip. The exact chemical forms of these oxides are still to be determined to answer this question.

SUMMARY

Stress corrosion cracking (SCC) behavior of three Ni-base alloys in a high temperature caustic environment was evaluated. Cross-sectional specimens of Alloy 625 have been specially prepared to evaluate the intergranular SCC crack tip microstructure and corrosion products inside the crack and near the crack tip using Analytical Electron Microscopy (AEM). In addition, Auger/ESCA evaluation of the crack facets and the general corrosion surfaces were performed for Alloys 625, 600 and 690. The Auger/ESCA and AEM results showed a Ni-rich de-alloying surface film on the general surface and inside the crack opening. This shows that general corrosion or intergranular attack (IGA) resistance in caustic should increase with increasing Ni level in these Ni-base alloys. It is in agreement with the potential-pH (Pourbaix) diagrams in general. These results also showed no Ni-rich de-alloying film, but Cr-rich oxides inside the crack tips. This suggests that SCC resistance should also be affected by the Cr level. A high Cr level along the grain boundary should improve the intergranular SCC resistance of these Ni-base alloys in caustic. This could explain the good SCC resistance in Alloy 690 because of its high Cr content. These results also support thermal treatment to increase Cr contents at grain boundaries to improve SCC resistance.

ACKNOWLEDGEMENTS

Drs. Tom Miller and Steve Ziemniak are gratefully acknowledged for many helpful discussions on the high temperature pH value calculation and oxide solubility. Mr. Nathan Lewis is acknowledged for sharing the Alloy 600 results. We are grateful for Mr. Paul Sander who performed the Auger/ESCA analysis. The technical assistance of Mr. Larry Zeglen and Mr. Alvah Fergerson is gratefully acknowledged. The Knolls Atomic Power Laboratory is operated for the U.S. Department of Energy under Contract No. DE-AC12-76SN00052.

REFERENCES

1. R. [illegible]den, "Corrosion Performance of Alloy 690," Proceedings: 1989 EPRI Alloy 690 Workshop, EPR[illegible]P-6750-SD, April 1990

2. A. J. Sedriks, et.al., "Inconel Alloy 690 - A new Corrosion Resistant Material, Corrosion Engineering (Boshoku Gijutsu), vol.28, No. 2, p. 82 (1979)

3. Ph. Berge and J. R. Donati, "Materials Requirements for Pressurized Water Reactor Steam Generator Tubing," Nuclear Technology, vol55, p.88 (1981)

4. S. J. Green, "Steam Generator Tube Material," EPRI Steam Generator Reference Book, Chap. 4 (1985)

5. R. B. Frank and T. A. Debold, "Properties of An Age-Hardenable, Corrosion-resistant, Nickel-Base Alloy," Corrosion 88, paper no. 75 (1988)

6. M. Sundararaman, et.al., "Precipitation of the o-Ni_3Nb Phase in Two Nickel Base Superalloys," Met. Trans. A., vol. 19A, p. 453 (1988)

7. A. R. McIlree and H. T. Michels, "Stress Corrosion Behavior of Fe-Cr-Ni and Other Alloys in High Temperature Caustic Solutions," Corrosion, vol.33, No.2, p.60 (1977)

8. J. B. Lumsden and P. J. Stocker, "Inhibition of IGA in Nickel Base Alloys in Caustic Solutions," Corrosion88, paper no. 252 (1988)

9. A. M. Lancha, et.al., "Auger/ESCA Analysis of Inconel 600 Tested in Caustic and Acidic Environments," EPRI Steam Generator IGA/SCC Workshop, Dec. 8-10, 1992

10. N. Lewis, et.al.,"Cross Sectional AEM Analysis of SCC Cracks," EPRI Steam Generator IGA/SCC Workshop, Dec. 8-10, 1992

11. P. L. Daniel and S. L. Harper, "Use of Pourbaix Diagrams to Infer Local Pitting Conditions," EPRI NP-4831, October 1986

12. J. A. Gorman, "Effects of Corrosion Potential on IGA/SCC," EPRI Crevice Chemistry Workshop, June 28-29, 1993

13. S. E. Ziemniak, "Metal Oxide Solubility Behavior in High Temperature Aqueous Solutions," Journal of Solution Chemistry, Vol. 21, No. 8, p. 745 (1992)

14. P. L. Andresen, "Modeling of Water and Material Chemistry Effects on Crack Tip Chemistry and Resulting Crack Growth Kinetics," Proceedings of the Third International Symposium on Environmental Degradation of Materials in Nuclear Power Systems - Water Reactors, August 30 - September 3, 1987, Traverse City, Michigan, USA

15. R. W. Staehle, "Understanding 'Situation-Dependent Strength': A Fundamental Objective in Assessing the History of Stress Corrosion Cracking," Proceedings of the First International Conference on Environment-Induced Cracking of Metals, October 2-7, 1988, Kohler, Wisconsin, USA

16. J. B. Lee, "Elevated Temperature Potential-pH Diagrams for the Cr-H_2O, Ti-H_2O, Mo-H_2O, and Pt-H_2O Systems," Corrosion Vol. 37, No. 8, p. 467 (1981)

17. P. Paine, "IGA/SCC Inhibitors: Progress Report," EPRI 1993 Crevice Chemistry Workshop, June 28-30, 1993

TABLE 1

CHEMICAL COMPOSITION OF ALLOYS 625, 600 AND 690 MATERIALS (wt %)

Material	Heat	C	Mn	Si	P	S	Cr	Mo	Nb	Fe	Ti	Al	Co	Ni
Alloy 625 tube	A	0.030	0.10	0.20	0.012	0.003	21.86	9.00	3.50	4.02	-	0.20	-	bal.
Alloy 625 Plate	B	0.010	0.21	0.21	0.012	0.001	22.47	8.51	3.54	3.85	0.22	0.16	-	bal.
Alloy 690 tube	C	0.029	0.14	0.20	0.001	0.001	29.20	-	-	7.90	0.19	0.25	0.08	bal.
Alloy 600 tube	D	0.042	0.19	0.22	0.005	0.002	15.29	-	-	8.36	0.17	0.14	0.05	bal.

TABLE 2

THERMAL HISTORY OF MATERIALS AND TEST RESULTS AFTER 500 HOURS EXPOSURE

Material	Heat	Thermal Treatment	Stress Relief	Average Maximum Crack Depth	
				μm	(mils)
Alloy 625 tube	A	-	566°C (1050F)/7hr	439	(17.3)
Alloy 600 tube	C	-	607°C (1125F)/7hr	137	(5.4)
Alloy 690 tube	D	1052°C (1925F)/4hr + 718°C (1325F)/10hr	607°C (1125F)/7hr + 566°C (1050F)/7hr	58	(2.3)
Alloy 625 plate	B	1093°C (2000F)/24hr + 871°C (1600F)/8hr + 649°C (1200F)/24 hr	566°C (1050F)/7hr	1232	(48.5)

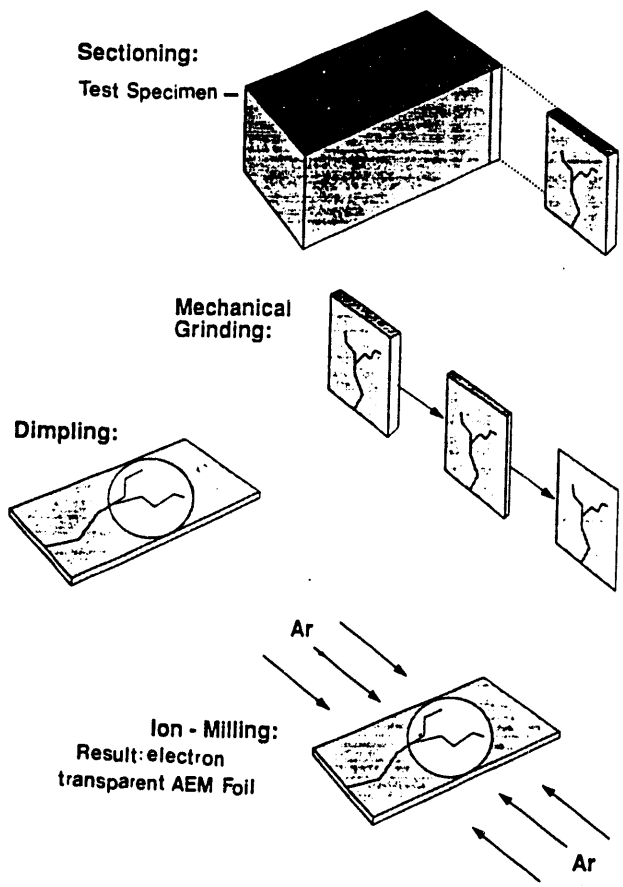

Figure 1 - AEM Sample Preparation

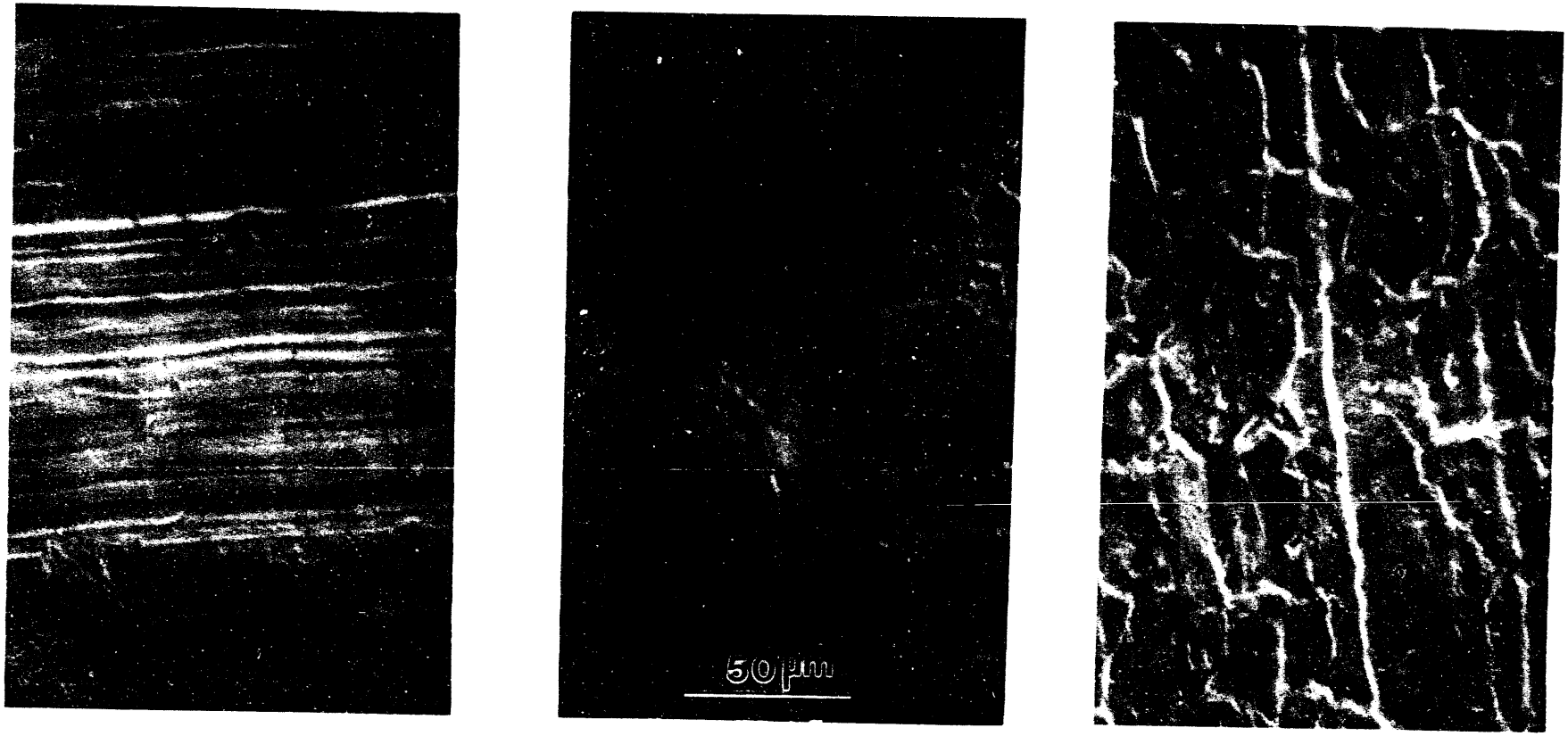

(a) (b) (c)

Figure 2: SEM Micrographs of SCC Specimens Showing General Surface Features After 500 Hours Exposure in 10% Caustic at 585°F. (a) A600 (b) A690 and (c) A625

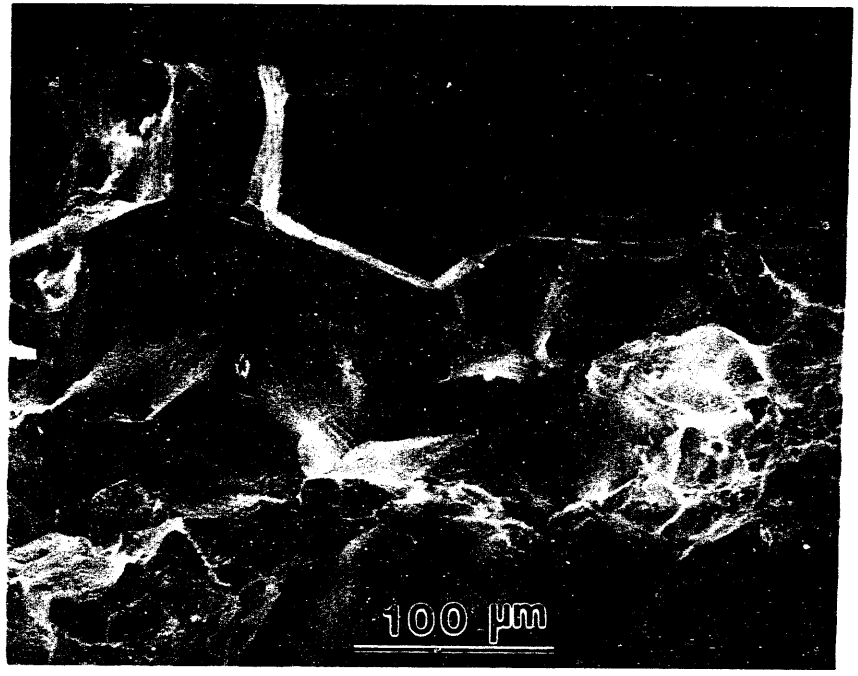

Figure 3: SEM Micrographs of A625 Specimen Showing Intergranular Cracking and Corrosion Products on Crack Facets After 500 Hours Exposure in 10% Caustic at 585°F

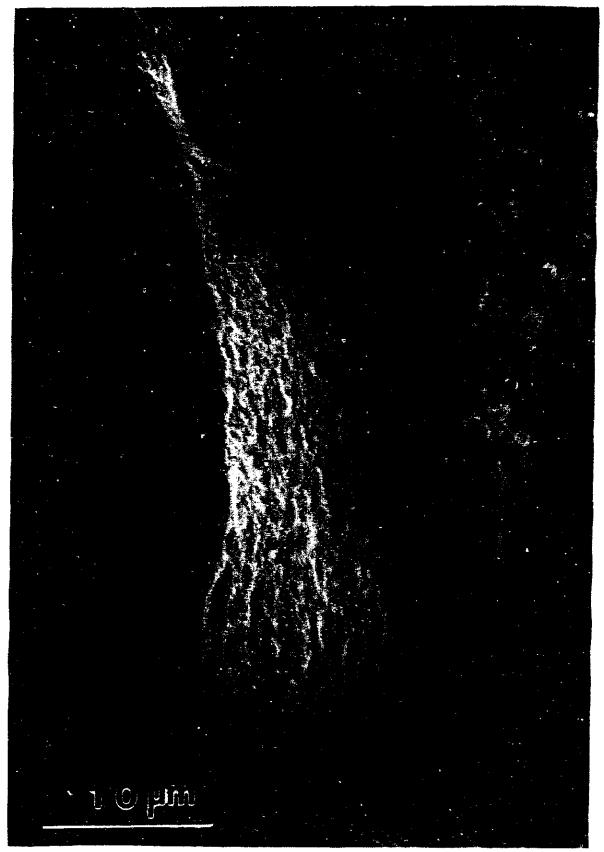

(a)

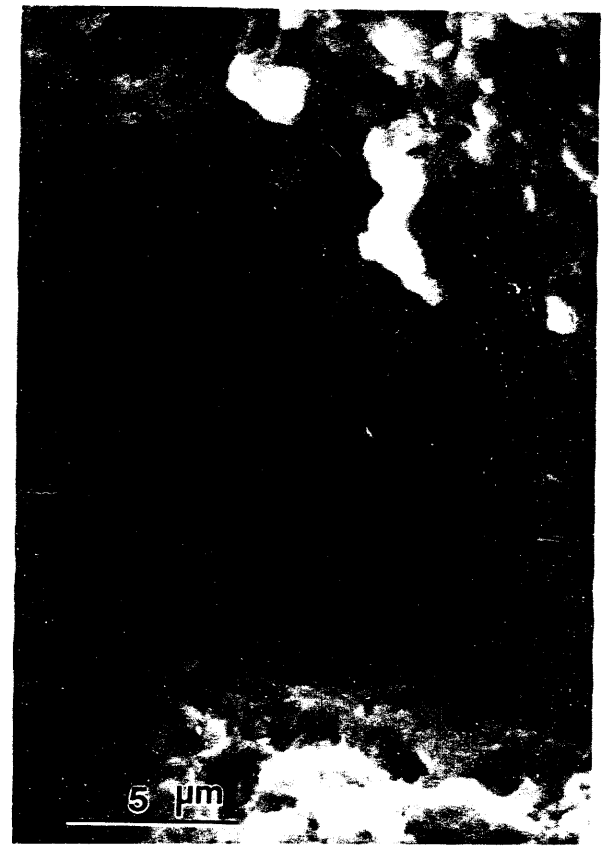

(b)

Figure 4: SEM Fractography of A625 Specimen Showing Fine Corrosion Products on Crack Facets. (a) 2,210X (b) 4,440X

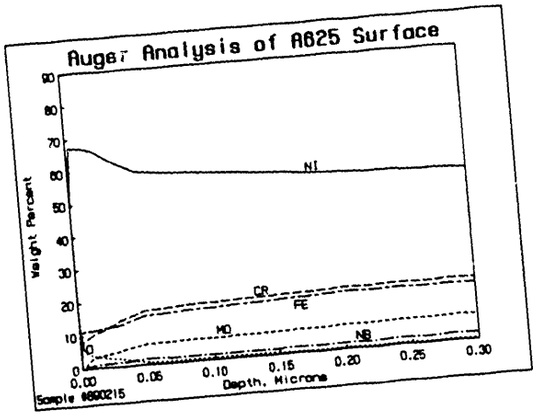

FIGURE 5 - Auger Analysis of General Surface for Alloy 625 After 500 Hours Exposure in 10% Caustic at 585°F

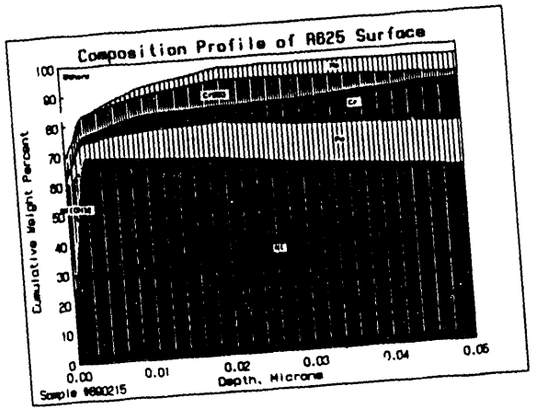

FIGURE 6 - ESCA Analysis of General Surface for Alloy 625 After 500 Hours Exposure in 10% Caustic at 585°F

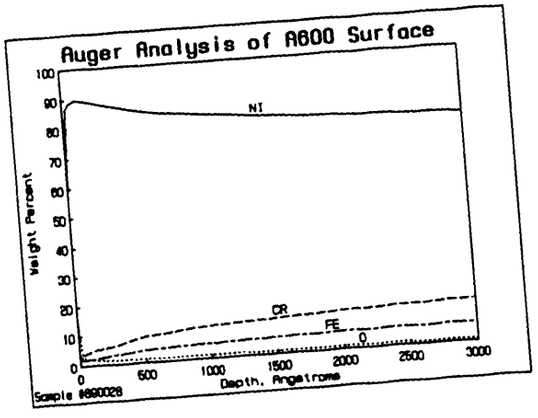

FIGURE 7 - Auger Analysis of General Surface for Alloy 600 After 500 Hours Exposure in 10% Caustic at 585°F

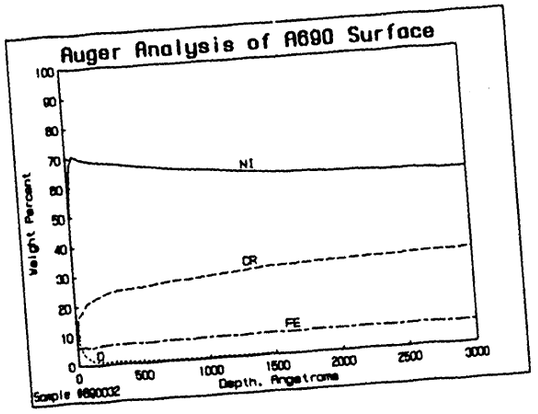

FIGURE 8 - Auger Analyses of General Surface for Alloy 690 After 500 Hours Exposure in 10% Caustic at 585°F

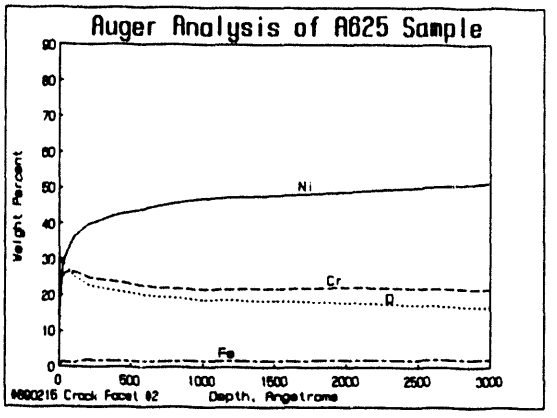

FIGURE 9 (a) - Auger Analysis of Crack Facet Near the Crack Tip of Alloy 625 After 500 Hours Exposure in 10% Caustic at 585°F

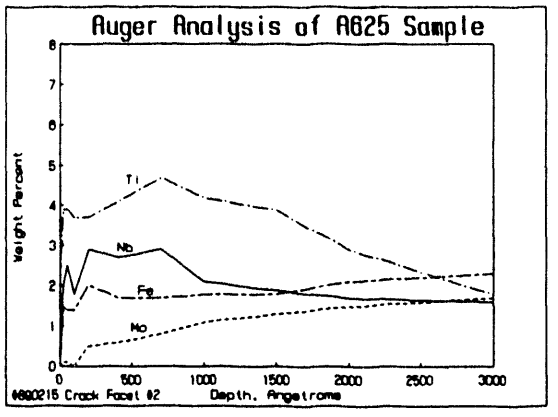

FIGURE 9 (b) - Same as 9 (a) but showing Ti, Nb, Fe and Mo Profiles

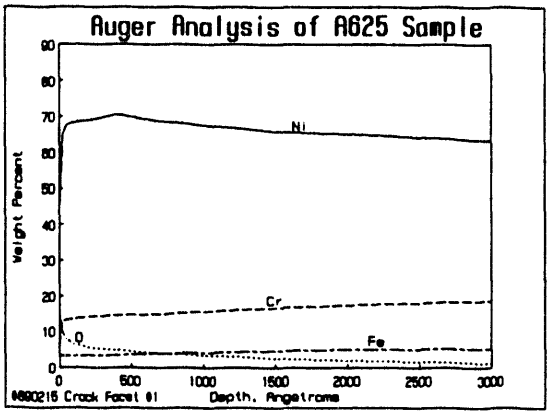

FIGURE 10 (a) - Auger Analysis of Crack Facet Near the Crack Opening of Alloy 625 After 500 Hours Exposure in 10% Caustic at 585°F

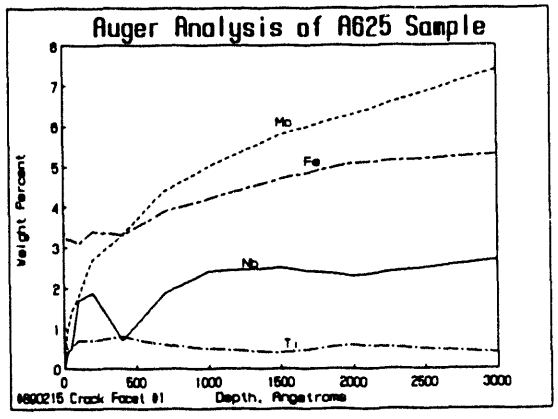

FIGURE 10 (b) - Same as 10 (a) But Showing Mo, Fe, Nb and Ti Profiles

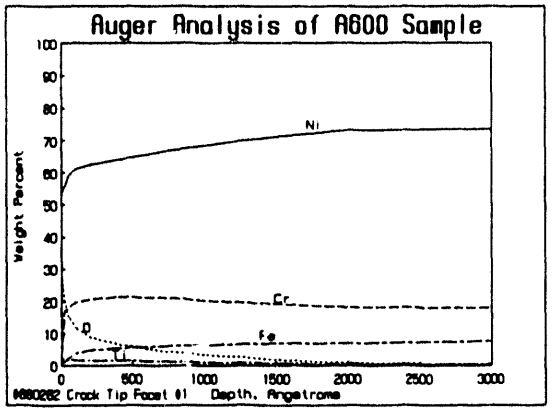

FIGURE 11 - Auger Analysis of Crack Facet Near the Crack Tip of Alloy 600 After 500 Hours Exposure in 10% Caustic at 585°F

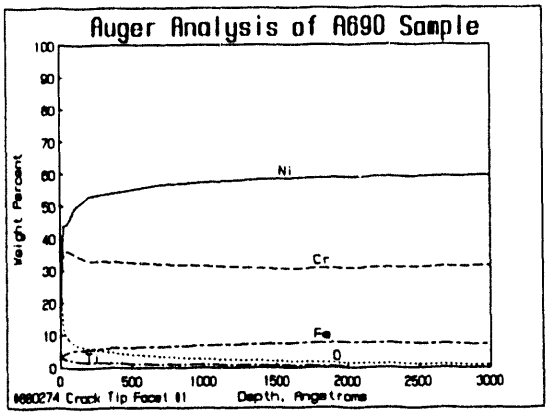

FIGURE 12 - Auger Analyses of Crack Facet Near the Crack Tip of Alloy 690 After 500 Hours Exposure in 10% Caustic at 585°F

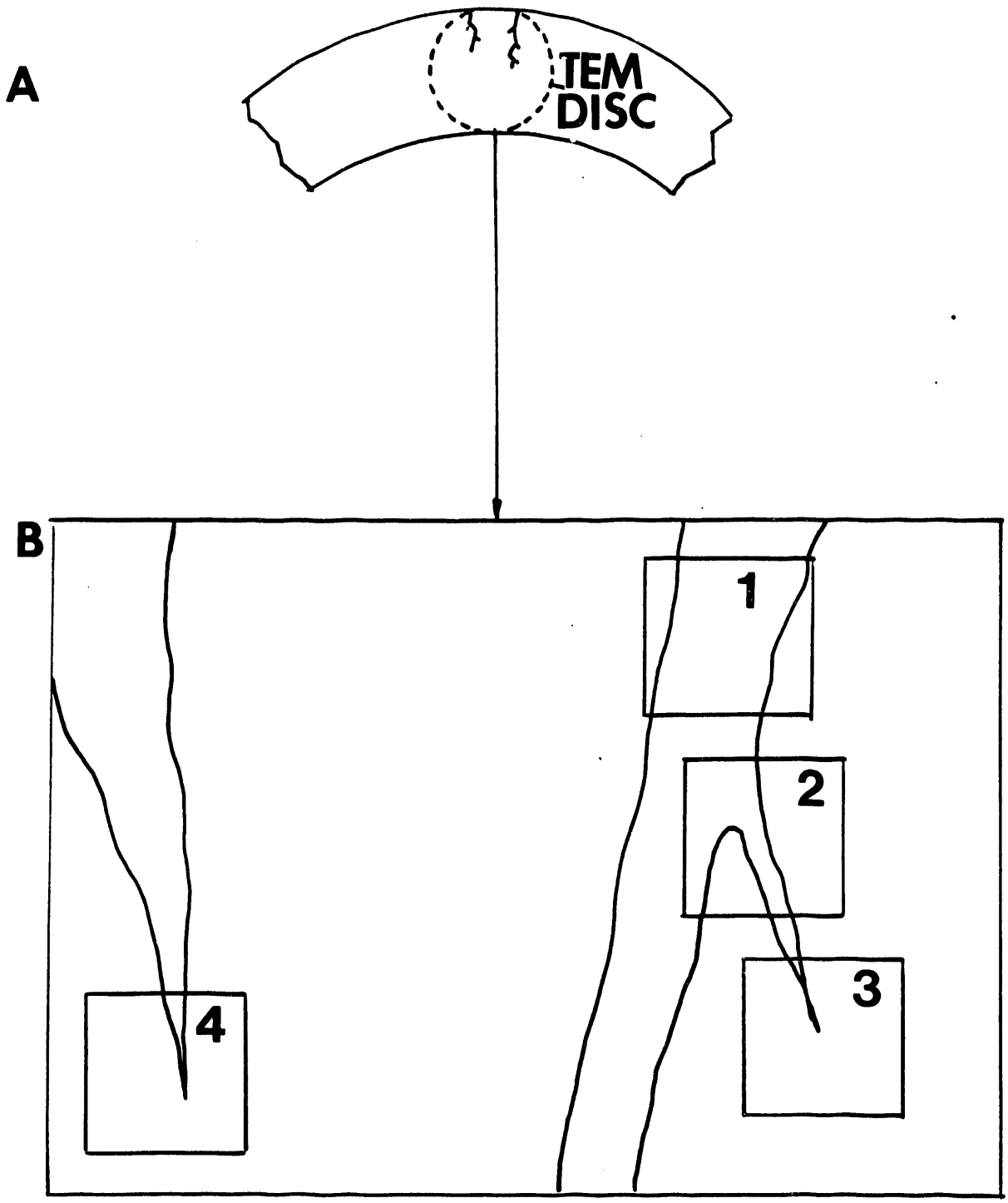

Figure 13: A. An Illustration of TEM Specimen Selection from a SCC-cracked A625 Sample

B. Crack-tip Regions Revealed in the Electron Transparent Area

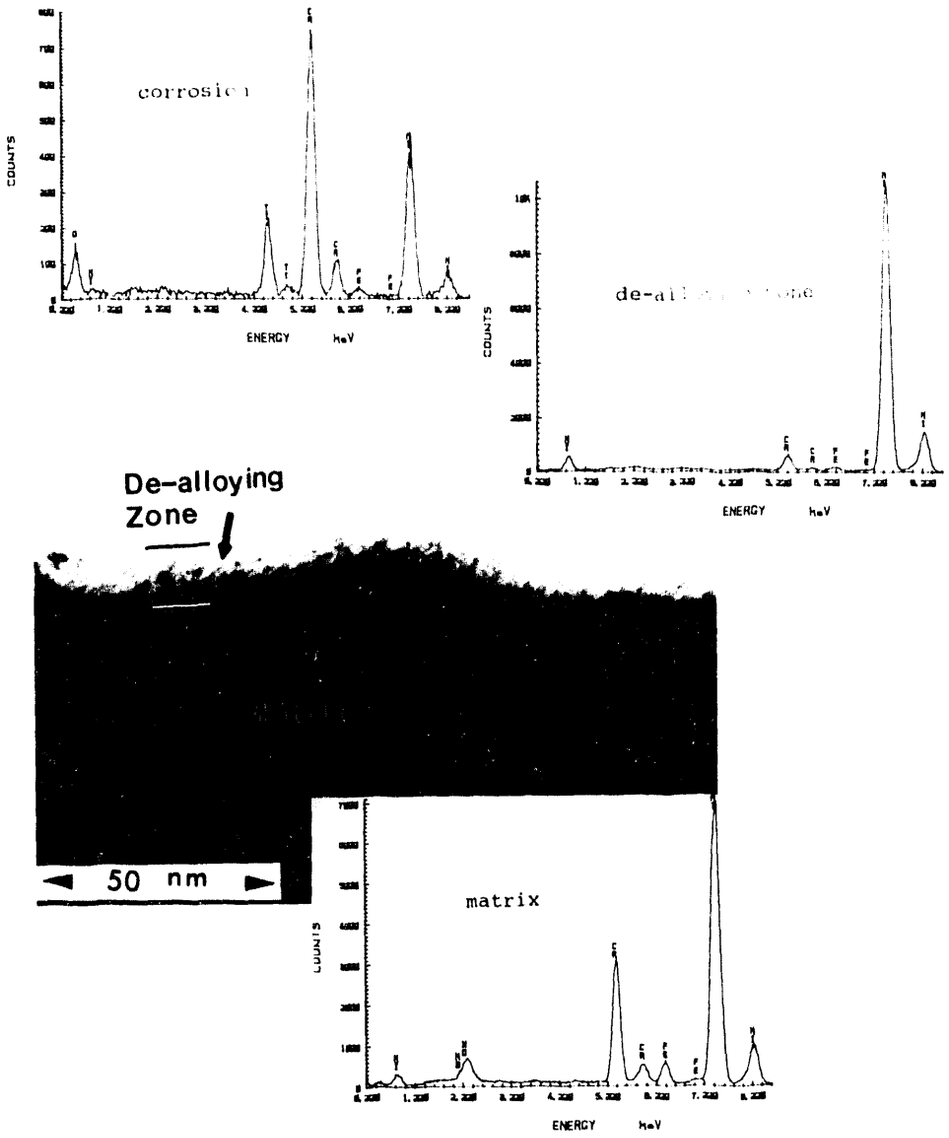

Figure 14: De-alloying Layer on Crack Surface in Crack Opening (Region 1)

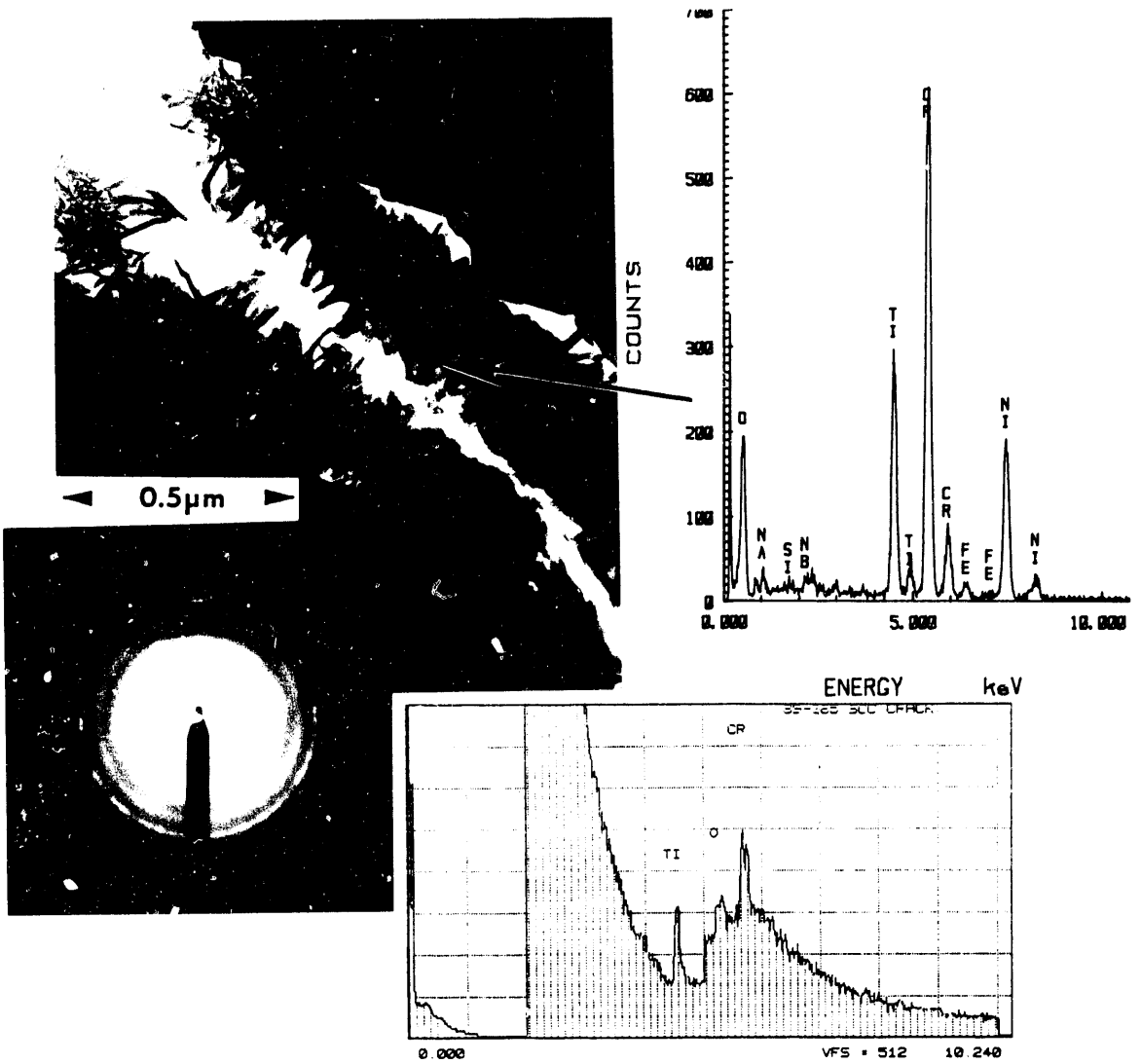

Figure 15: Oxide Appearance in the Crack Opening (Region 1)

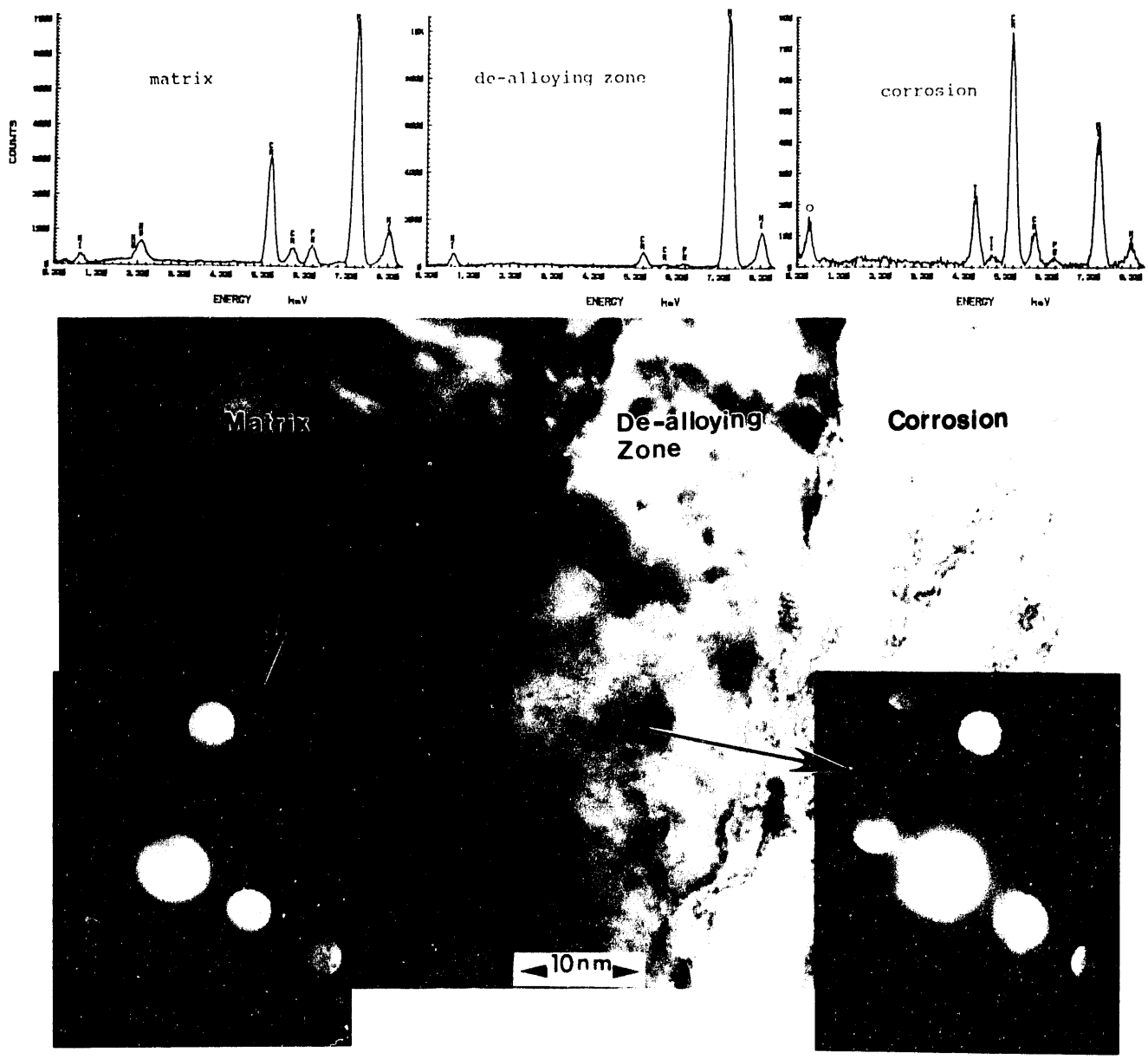

Figure 16: Microdiffraction Patterns and EDX Spectra of the De-alloying Layer in Mid Crack (Region 2)

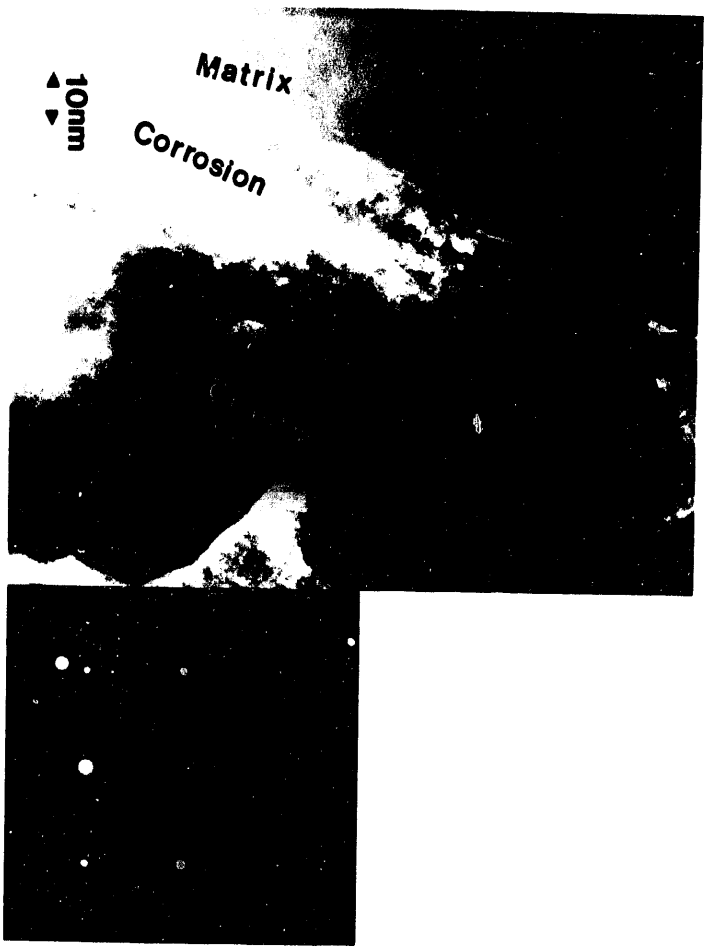

Figure 17: Lattice Image of Precipitate $Cr_{23}C_6$ in the Midst of Corrosion Products in Mid Crack (Region 2)

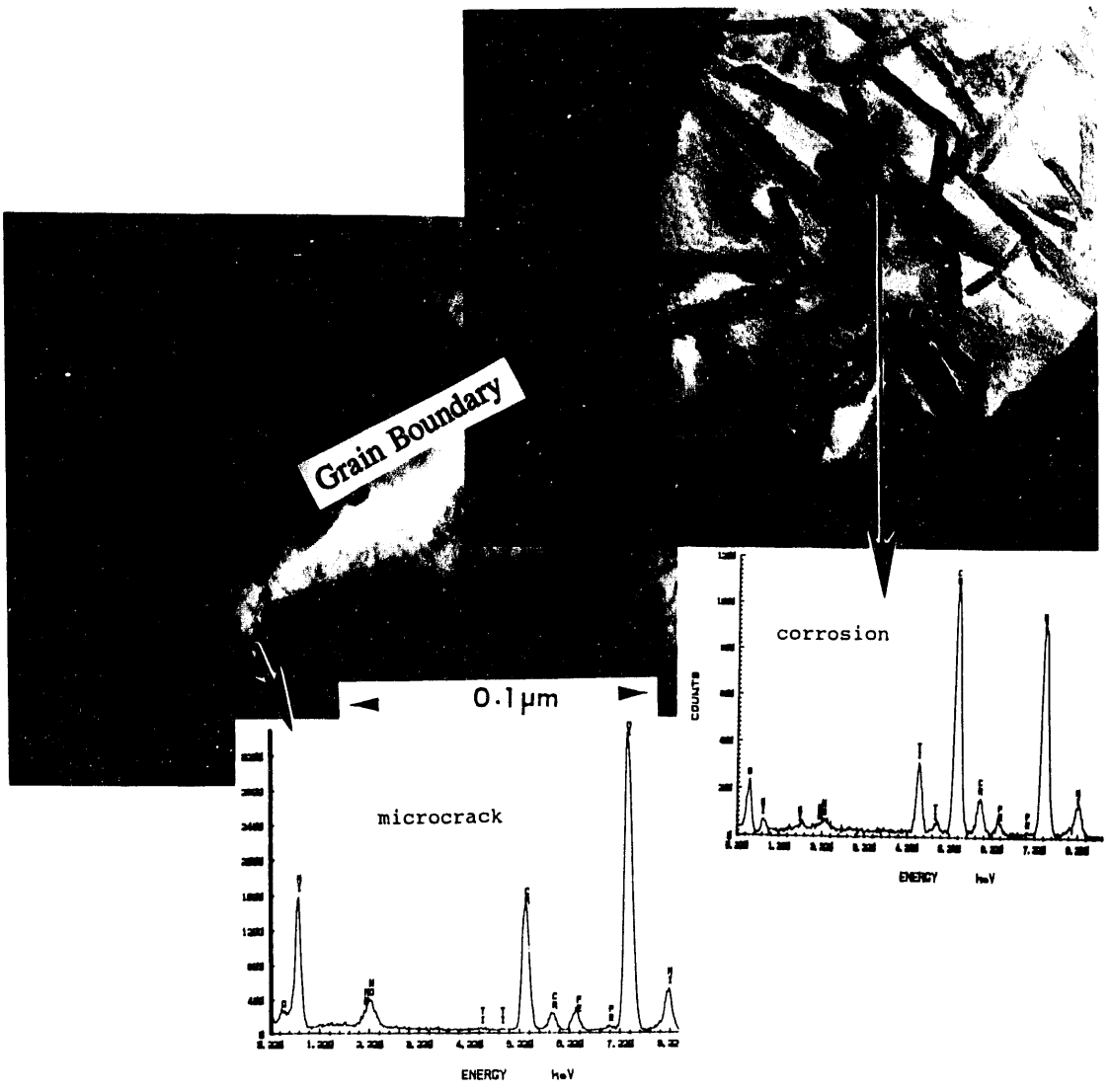

Figure 18: The Secondary Crack-tip (Region 3). The Arrows are Pointing Out the Microcracks (Cavities) at Grain Boundary Ahead of the Crack Tip

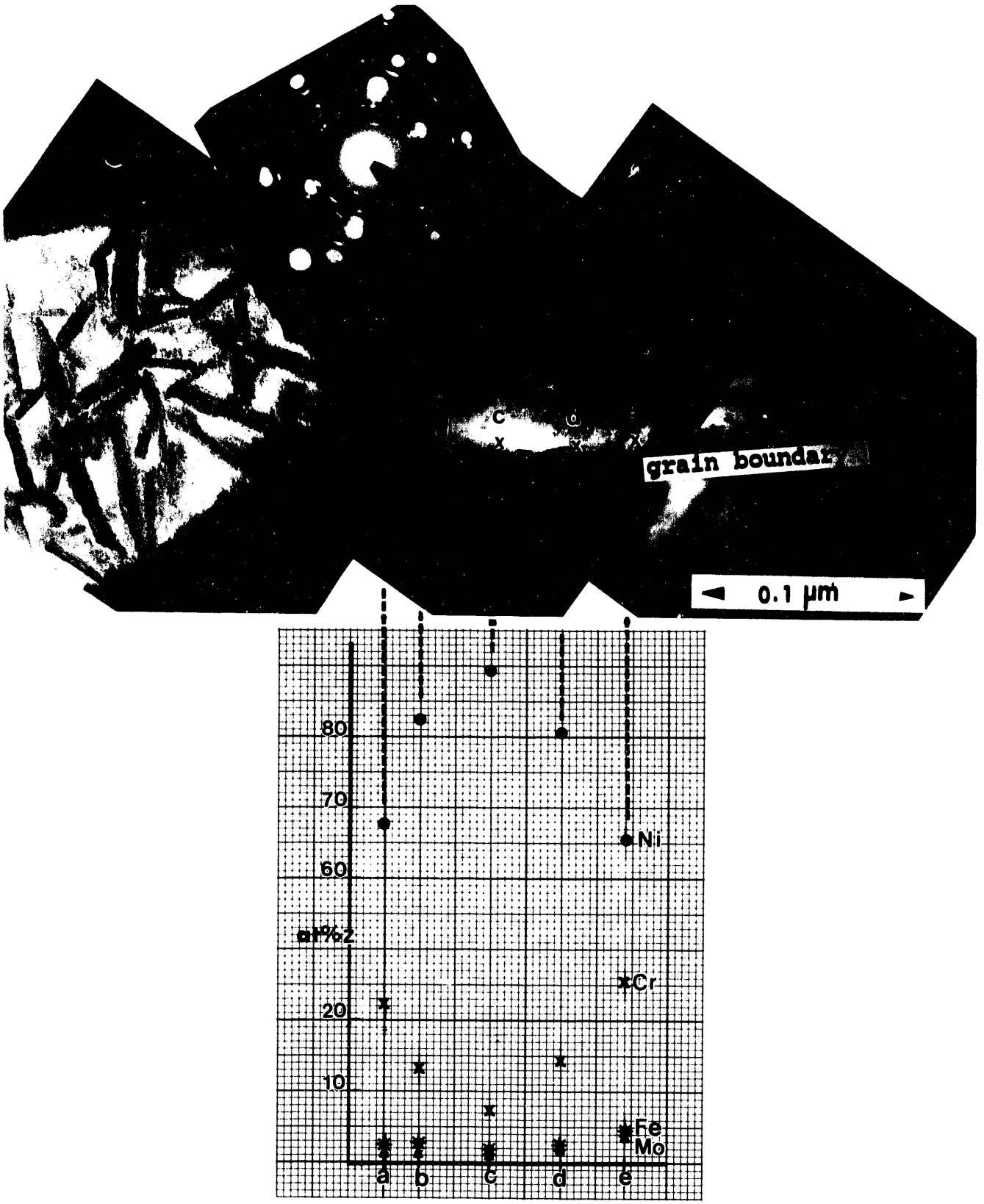

Figure 19: Results of EDX Measurements Along the Grain Boundary Ahead of the Secondary Crack Tip (Region 3)

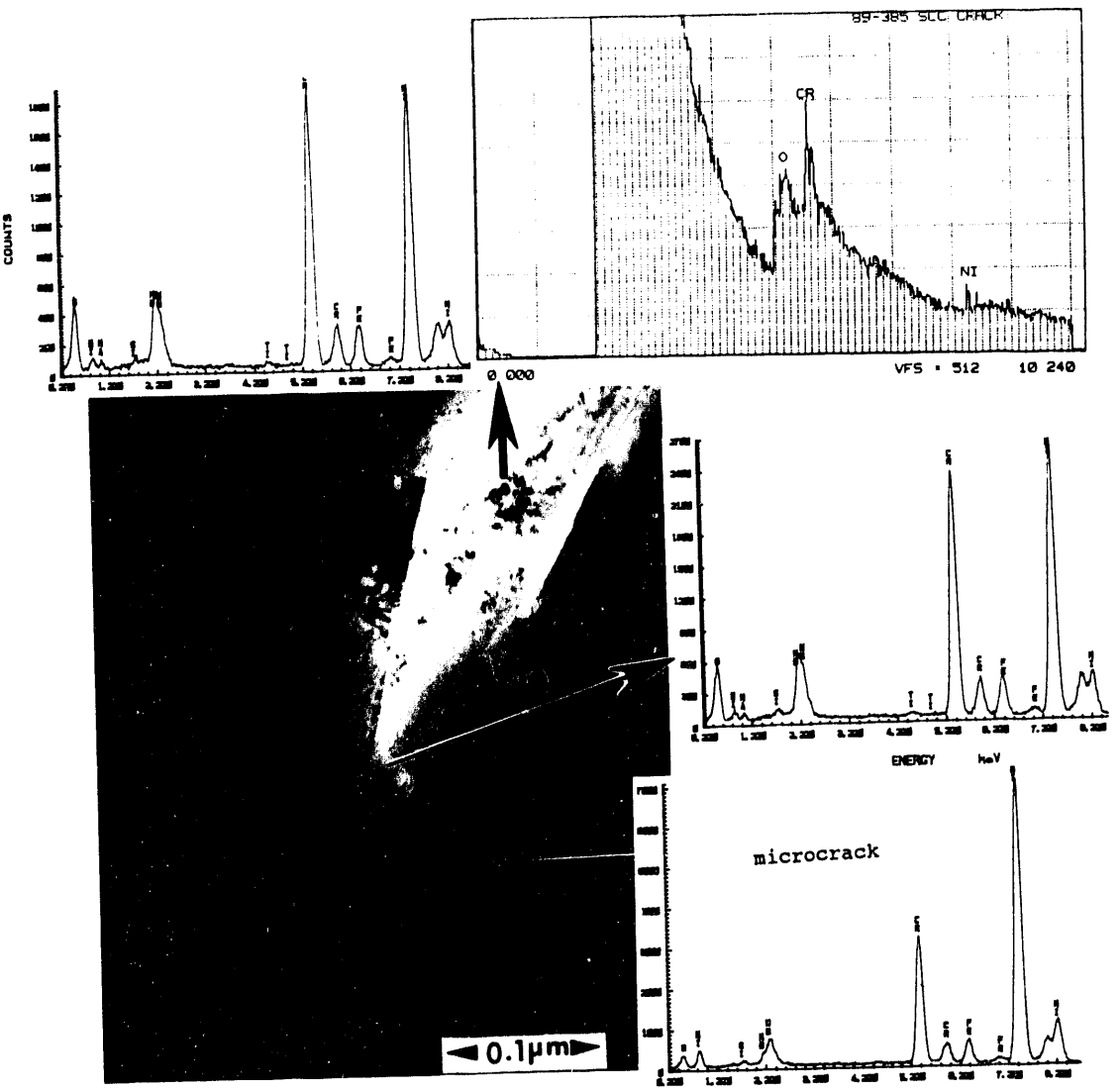

Figure 20: The Crack-tip Region of a Primary Crack in Region 4. The Arrows are Pointing Out the Microcracks (Cavities) at Grain Boundary Ahead of the Crack Tip

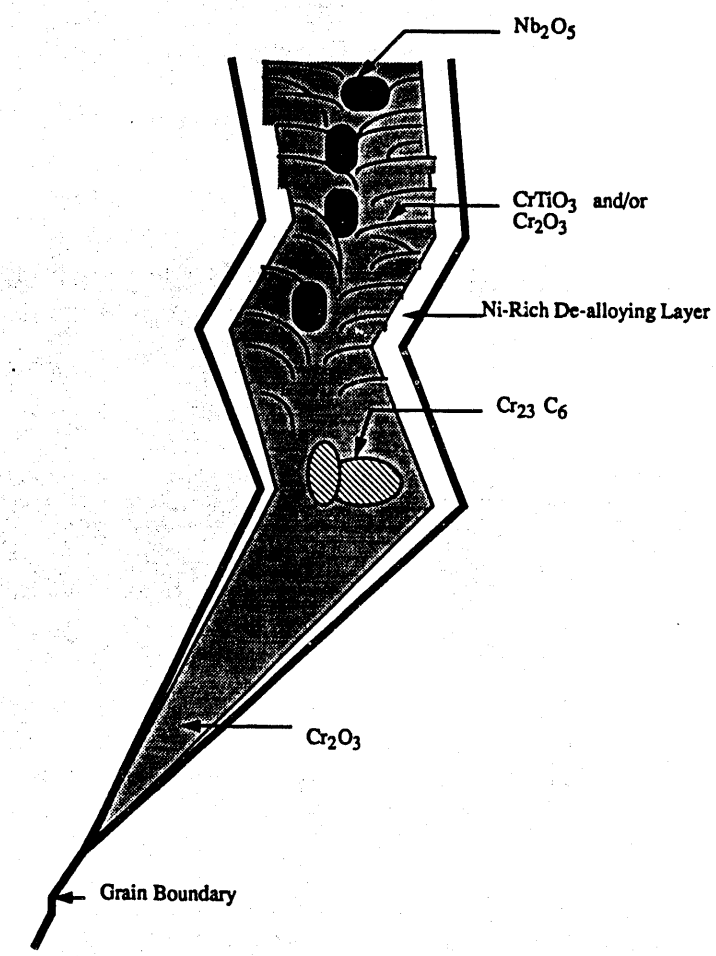

FIGURE 21 - Summary of Crack Tip Microstructure in a 10% Caustic Exposed Alloy 625 Specimen

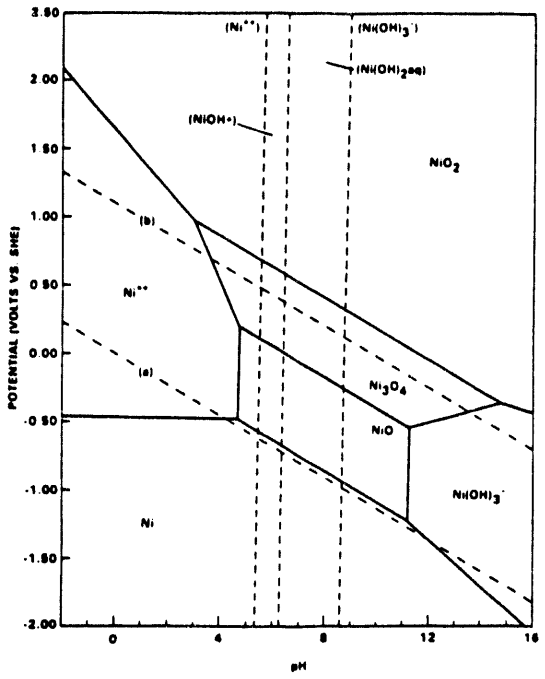

FIGURE 22 - Potential-pH Diagram for Nickel-Water System at 288°C with Dissolved Species Activities of 10^{-6} Showing Corrosion Modes (from Reference 11)

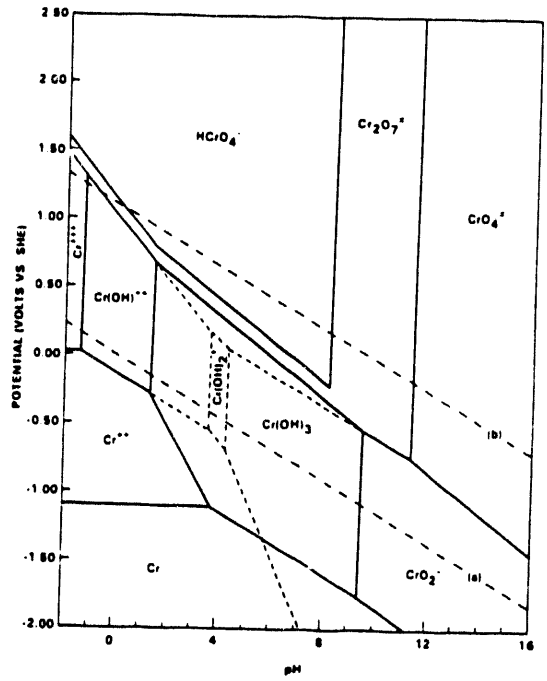

FIGURE 23 - Pourbaix Diagram for the Chromium-Water System at 288°C with Dissolved Species Activities of 10^{-3} (from Reference 11)

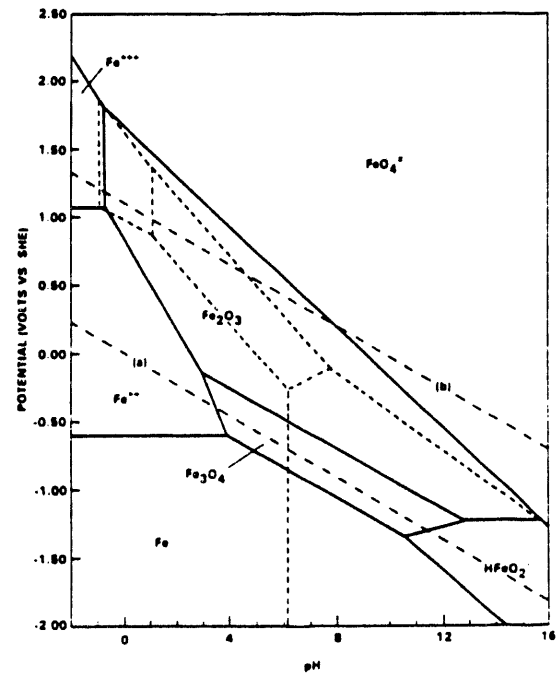

FIGURE 24 - Pourbaix Diagram for the Iron-Water System at 288°C with Dissolved Species Activities of 10^{-3} (from Reference 11)

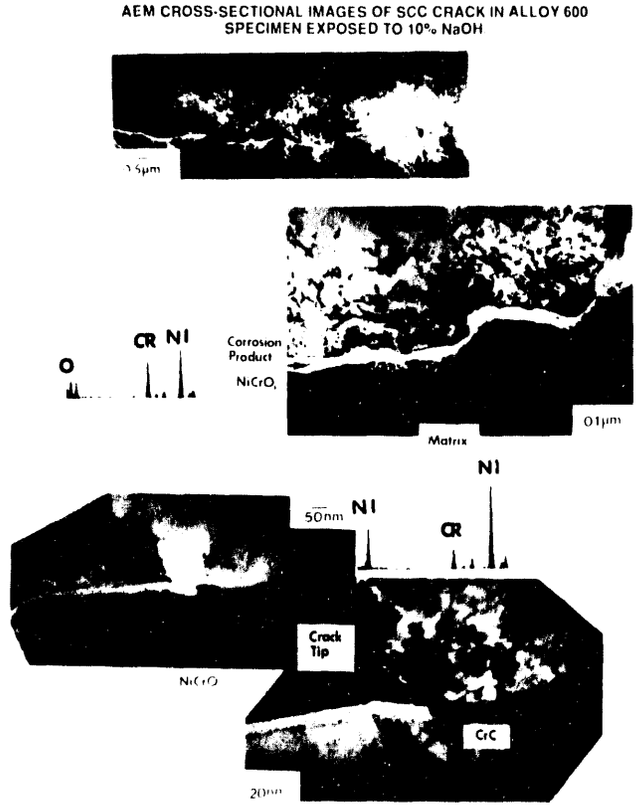

FIGURE 25 - Oxides and Crack Tip Microstructure in a 10% Caustic Exposed Alloy 600 Specimen.
(Courtesy of N. Lewis from Reference 10)

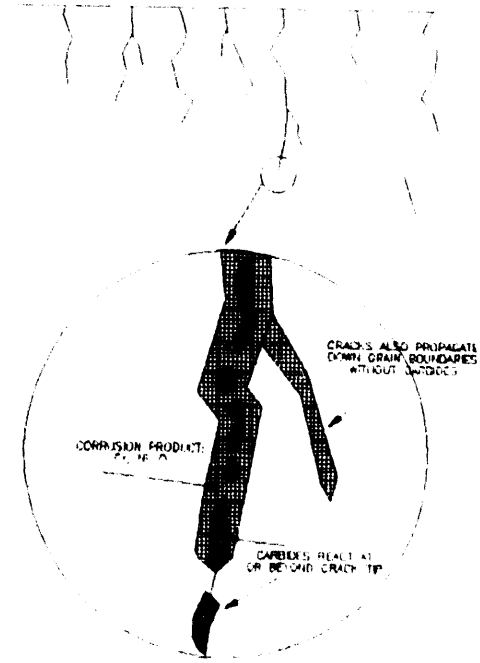

FIGURE 26 - A Summary of Crack-tip Microstructure in Alloy 600
(From Reference 10)

DATE
FILMED
8/25/94
END